nature climate change

Supplementary information

https://doi.org/10.1038/s41558-024-02115-x

Global patterns and drivers of tropical aboveground carbon changes

In the format provided by the authors and unedited

Table of contents:

Supplementary Tables

Table S1: The predictor variables used in the Boosted Regression Tree model for explaining spatial variability and trends in AGC gains.

Supplementary Figures

Fig. S1. Ecoregion map of the final study domain.

Fig. S2. Land cover fraction for forest, shrub, and grass/crop over the tropics.

Fig. S3. Ratio of AGC loss from deforestation (def.), other degradation, and edge effects to total non-fire forest AGC losses.

Fig. S4. Spatially comparison of AGC losses with gains over the tropics and three tropical continents.

Fig. S5. Maps of forest age (a), intact forest landscapes (b), and undisturbed forests (c).

Fig. S6. Temporal patterns of AGC changes over the tropics undisturbed forest from 2010–2020.

Fig. S7. Comparison of aboveground biomass carbon (AGC) estimates between Ometto and L-VOD for the year 2016.

Fig. S8. Interannual variability of global atmospheric CO_2 growth rate (CGR) and tropical AGC fluxes.

Fig. S9. AGC loss rates due to edge effects.

Fig. S10. Spatial patterns of AGC gains from the reference and BRT model.

Fig. S11. Spatial patterns of trends in AGC gains from the reference and BRT model.

Fig. S12. Soil moisture comparison between ERA5-Land (ERA5-L) and another global 1km products (Zheng et al., 2023).

Supplementary References

Table S1. The predictor variables used in the Boosted Regression Tree model for explaining spatial variability and trends in AGC gains.

Input factors		Spatial resolution	Time period	Sources
Spatial pattern	Trends			
T_a (°C)	δT_a (°C yr^{-1})	0.1°	2010–2020	ERA5-L
R_s (W m^{-2})	δR_s (W m^{-2} yr^{-1})	0.1°	2010–2020	ERA5-L
VPD (kPa)	δVPD (kPa yr^{-1})	0.1°	2010–2020	ERA5-L
SM (%)	δSM (% yr^{-1})	0.1°	2010–2020	ERA5-L
FRP (GW)	δFRP (GW yr^{-1})	1 km	2010–2020	MCD14DL
Forest fire (ha)	δforest fire (ha yr^{-1})	30 m	2010–2020	TMF
Human footprint (-)	δHFP (-)	1 km	2010–2020	Mu et al.
Livestock density (head/km²)	Livestock density (head/km²)	10 km	Static	FAO
Young plant. (ha)	δyoung plant. (ha yr^{-1})	30 m	2010–2020	Du et al.
Old plant. (ha)	δold plant. (ha yr^{-1})	30 m	2010–2020	Du et al.
Young rg (ha)	δyoung rg (ha yr^{-1})	30 m	2010–2020	TMF
Old rg (ha)	δold rg (ha yr^{-1})	30 m	2010–2020	TMF
Clay (%)	Clay (%)	250 m	Static	SoilGrids
SOC (t ha^{-1})	SOC (t ha^{-1})	250 m	Static	SoilGrids
Nitrogen (g kg^{-1})	Nitrogen (g kg^{-1})	250 m	Static	SoilGrids
Species (-)	Species (-)	500 m	Static	Sabatini et al.
F_t (%)	F_t (%)	10 m	2020	ESA2020
F_s (%)	F_s (%)	10 m	2020	ESA2020
F_g (%)	F_g (%)	10 m	2020	ESA2020
\	T_a (°C)	0.1°	2010–2020	ERA5-L
\	R_s (W m^{-2})	0.1°	2010–2020	ERA5-L
\	VPD (kPa)	0.1°	2010–2020	ERA5-L
\	SM (%)	0.1°	2010–2020	ERA5-L

T_a is near-surface air temperature; R_s is shortwave solar radiation; *VPD* is vapor pressure deficit; *SM* is soil moisture; These four variables were obtained from ERA5-land (ERA5-L) products with a spatial resolution of 0.1° and monthly interval in NetCDF format, and the monthly values were further aggregated to annual values. *FRP* is fire radiative power, obtained from MODIS Thermal Anomalies/Fire locations products (MCD14DL) with 1 km resolution in Shapefile format. *Forest fire* is the forest-related burned area, which is calculated by overlaying the GFED burned area layer with TMF deforestation and degradation data in GeoTIFF format, with a spatial resolution of 30 m and annual interval. *Human footprint*, an index to express the pressure imposed on the eco-environment by changing natural landscapes and ecological processes, was obtained from Mu et al. (2022), with a spatial resolution of 1 km and annual interval in GeoTIFF format. The FAO *livestock density* expresses the global distribution of the total number of buffaloes, cattle, chicken, ducks, goats, horses, pigs and sheep for the year 2015, with a spatial resolution of 10 km in NetCDF format. *Young plant.* and *old plant*. are the areas of plantations

less than and more than 10 years old, respectively, derived from the global maps of planting years of plantations (Du et al., 2022), with a spatial resolution of 30 m and annual intervals in GeoTIFF format. *Young rg*. and old *rg*. are areas of forest regrowth less than and more than 10 years old, respectively, derived from the TMF regrowth data, with a spatial resolution of 30 m and annual intervals. *SOC*, *clay*, and *nitrogen* are soil organic carbon stocks, proportion of clay particles (< 0.002 mm) in the fine earth fraction, and total nitrogen at 0–30 cm depth, respectively, obtained from the SoilGrids250m products with a spatial resolution of 250 m in GeoTIFF format (Hengl et al., 2017). *Species* is the species richness for vascular plants at 500 m resolution in GeoTIFF format. F_t, F_s, and F_g are fractions of tree, shrub, and grass/crop, respectively, in each 0.25° cell, derived from 10 m ESA2020 land cover map in GeoTIFF format (Zanaga et al., 2021). All the datasets, except for the TMF that covers most of the tropical regions, are global maps, and we extracted the tropical maps and then aggregated them to 0.25° to match the resolution of L-VOD. The ERA5-L data are available at https://cds.climate.copernicus.eu/cdsapp#!/dataset/reanalysis-era5-land-monthly-means?tab=form. The MODIS MCD14DL data are available at https://www.earthdata.nasa.gov/learn/find-data/near-real-time/firms/mcd14dl-nrt. The SoilGrids data are available at https://www.isric.org/explore/soilgrids. The ESA2020 data are available at https://worldcover2020.esa.int/.

Fig. S1. Ecoregion map of the final study domain. The ecoregion data was obtained from Olson et al. (2001).

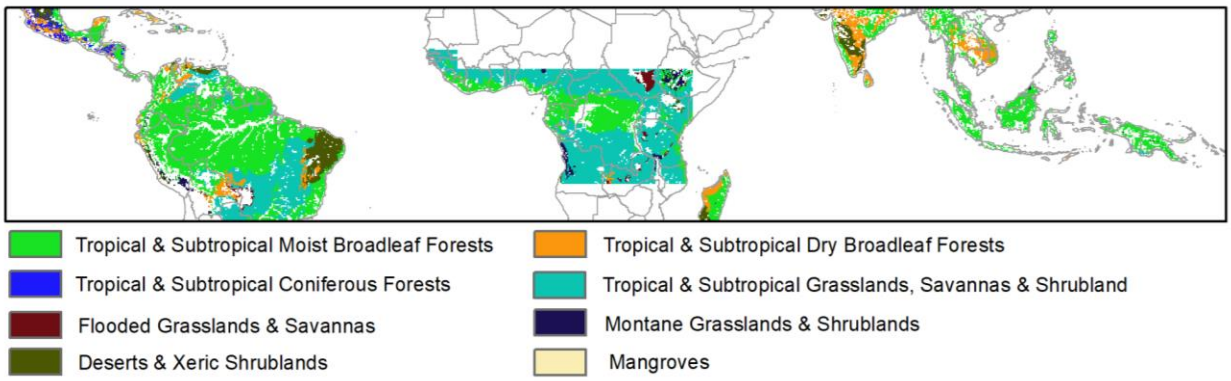

Fig. S2. Land cover fraction for forest, shrub, and grass/crop over the tropics. The land cover information was derived from the ESA WorldCover 2020 product (Zanaga et al., 2021).

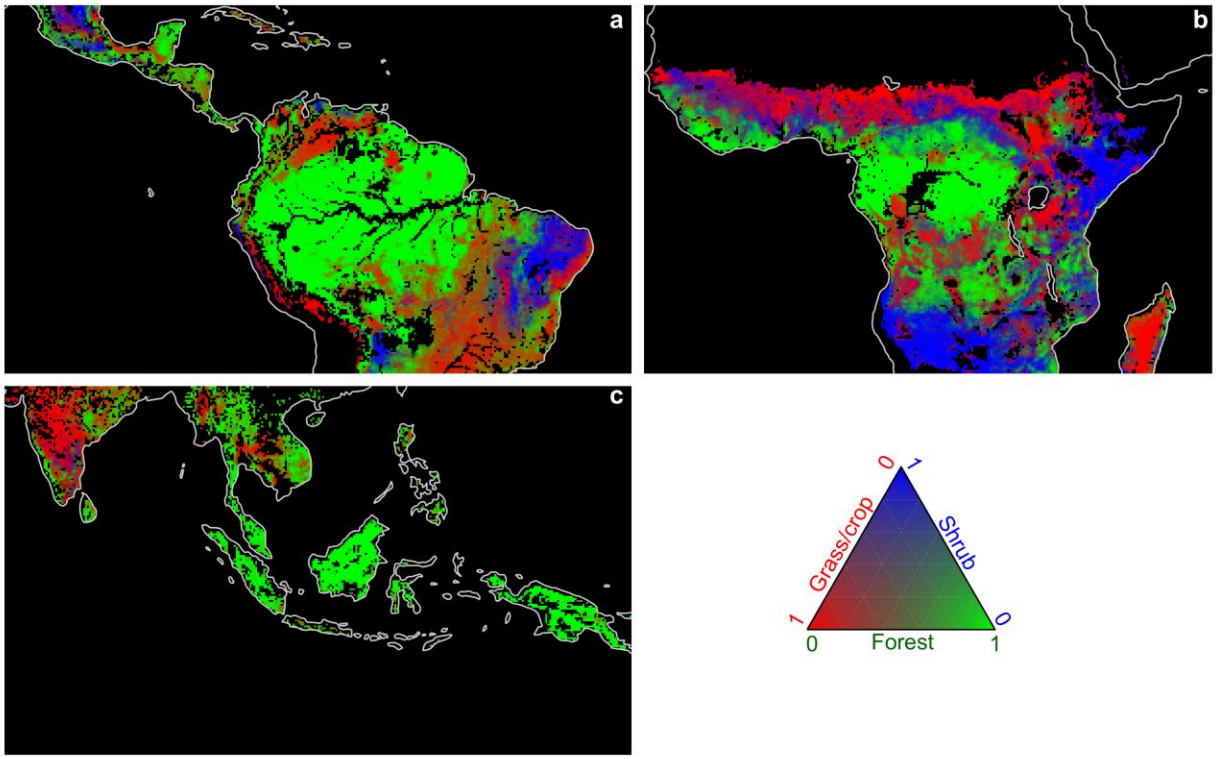

Fig. S3. Ratio of AGC loss from deforestation (def.), other degradation, and edge effects to total non-fire forest AGC losses.

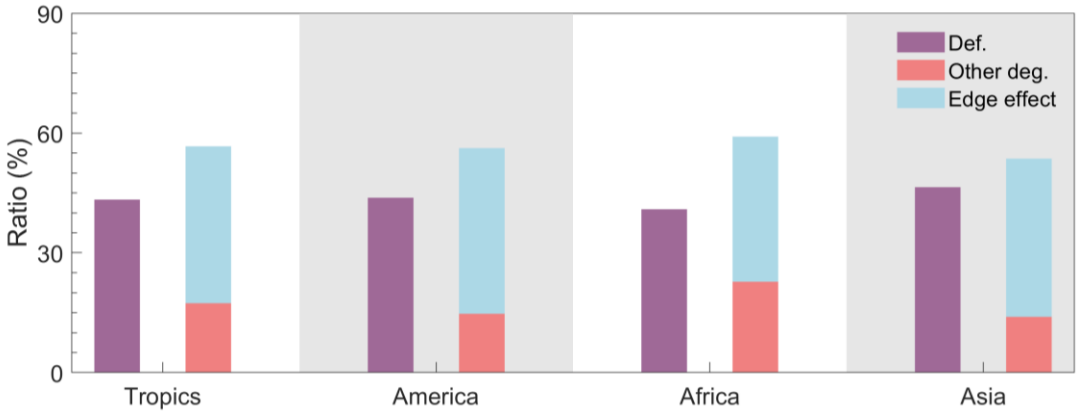

Fig. S4. Spatially comparison of AGC losses with gains over the tropics and three tropical continents. The p-values are calculated using a t-test.

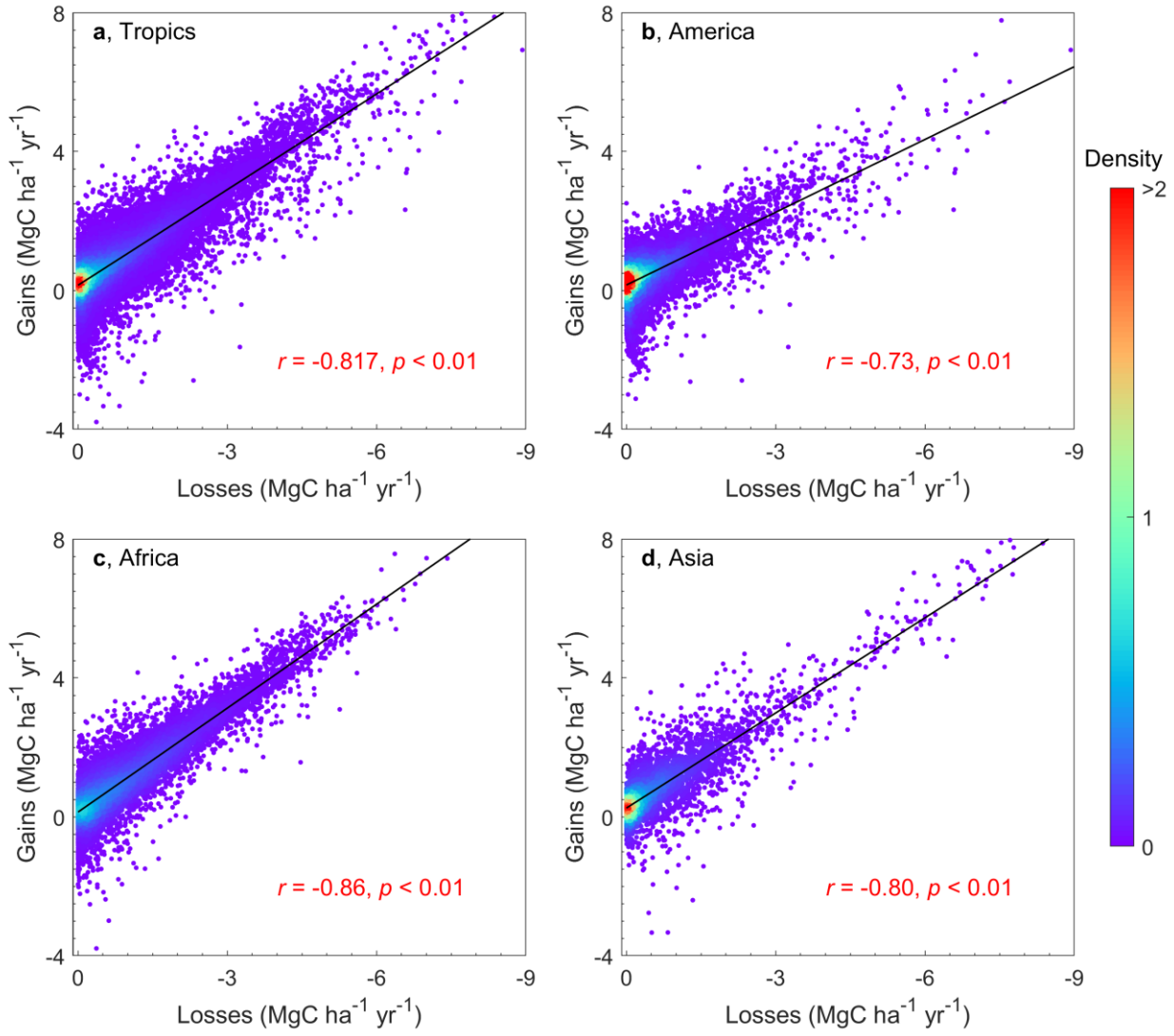

Fig. S5. Maps of forest age (a), intact forest landscapes (b), and undisturbed forests (c). Undisturbed forests are defined as forests with an age of more than 140 years and within intact forest landscapes (Yang et al., 2023). The forest age data were obtained from Besnard et al. (2021), and intact forest landscapes were obtained from Potapov et al. (2008).

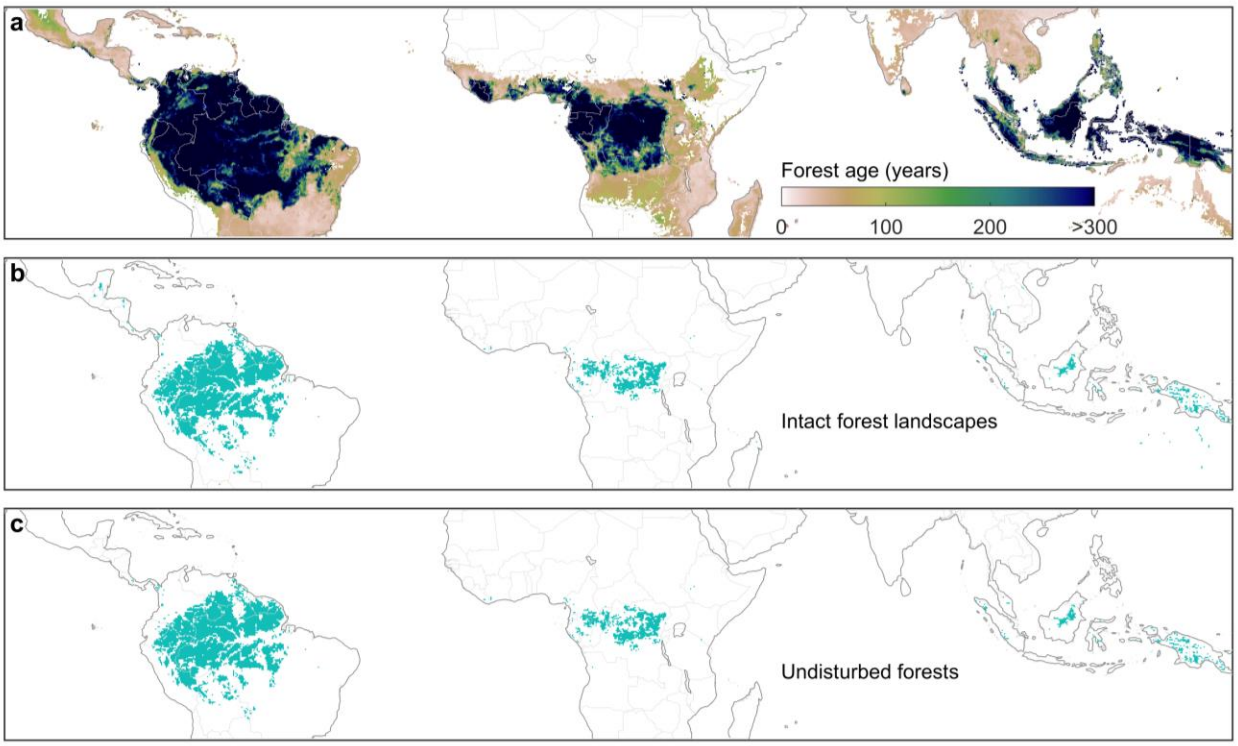

Fig. S6. Temporal patterns of AGC changes over the tropics undisturbed forest from 2010–2020. The solid lines indicate the mean values and shaded areas represent ±1 s.d. among the 18 estimates (see *Methods*).

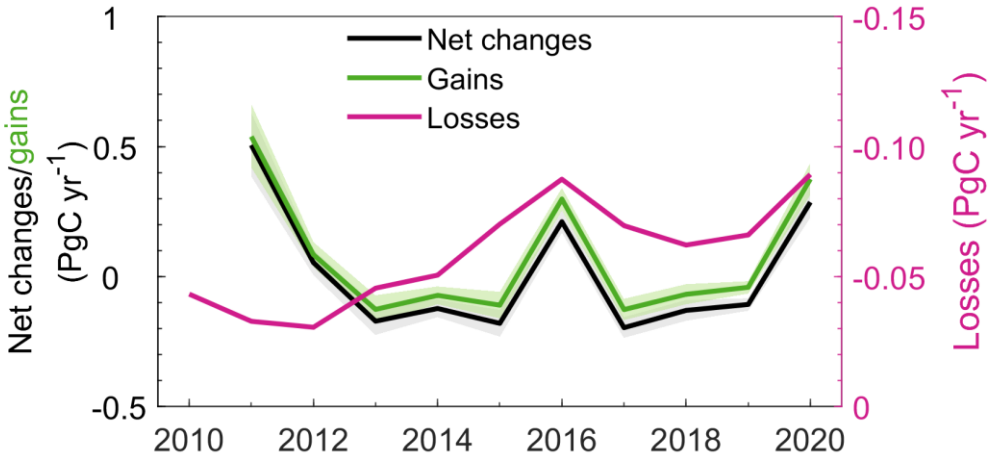

Fig. S7. Comparison of aboveground biomass carbon (AGC) estimates between Ometto and L-VOD for the year 2016. a-b, Spatial patterns of AGC from Ometto (**a**) and L-VOD (**b**). **c**, Scatterplot of AGC between Ometto and L-VOD. Ometto map refers to the AGC map created by Ometto et al. (2023).

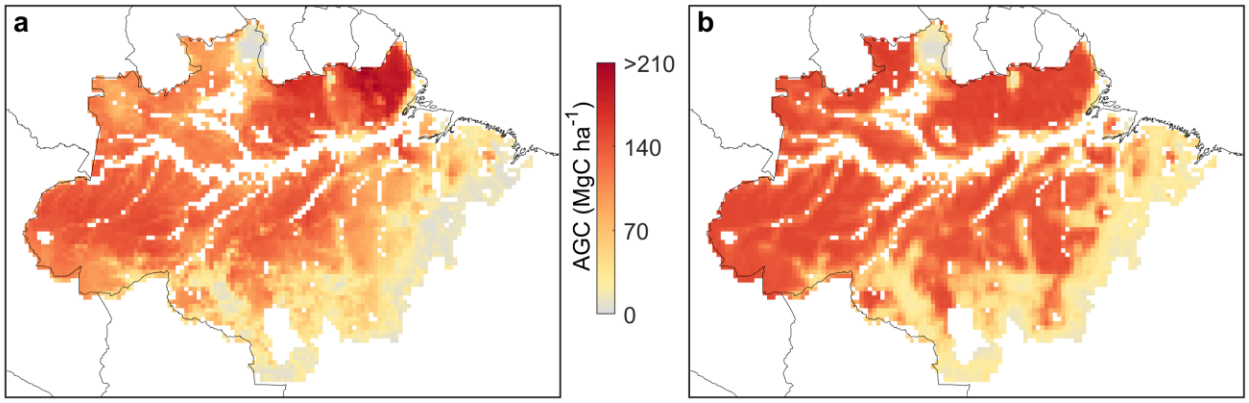

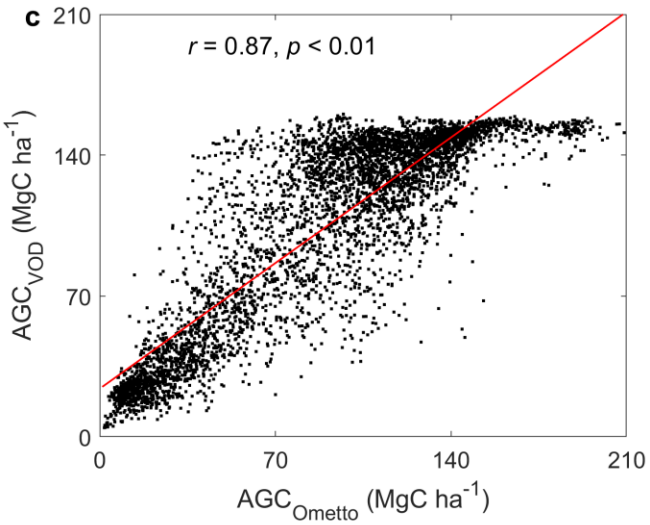

Fig. S8. Interannual variability of global atmospheric CO_2 growth rate (CGR) and tropical AGC fluxes. CGR was derived from the annual difference in atmospheric CO_2 concentration obtained from the National Oceanic and Atmospheric Administration. The shaded areas in grey represent the uncertainty of CGR; the shaded areas in red represent ±1 s.d. among the 18 estimates of AGC fluxes (see *Methods*). The p-values are calculated using a t-test.

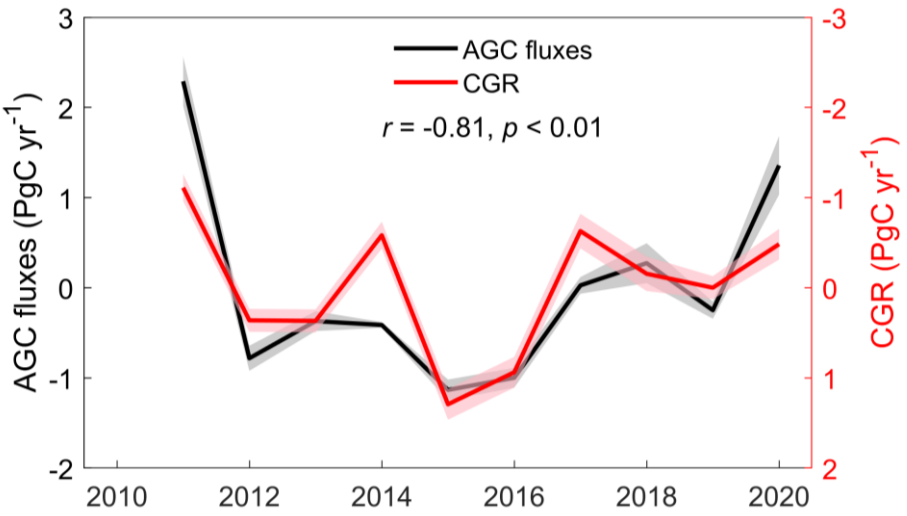

Fig. S9. AGC loss rates due to edge effects. The loss rate data were obtained from Silva Junior et al. (2020).

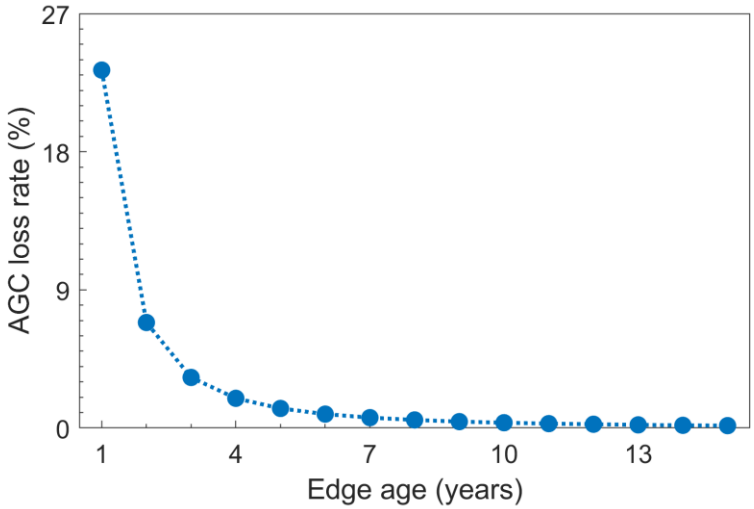

Fig. S10. Spatial patterns of AGC gains from the reference and BRT model. a, AGC gains from the reference, **b** AGC gains from the BRT model. **c**, Accuracy of the BRT model for predicting the signs of AGC gains. In the inset of **c**, T, AM, AF, and AS denotes the tropics, tropical America, tropical Africa, and tropical Asia, respectively.

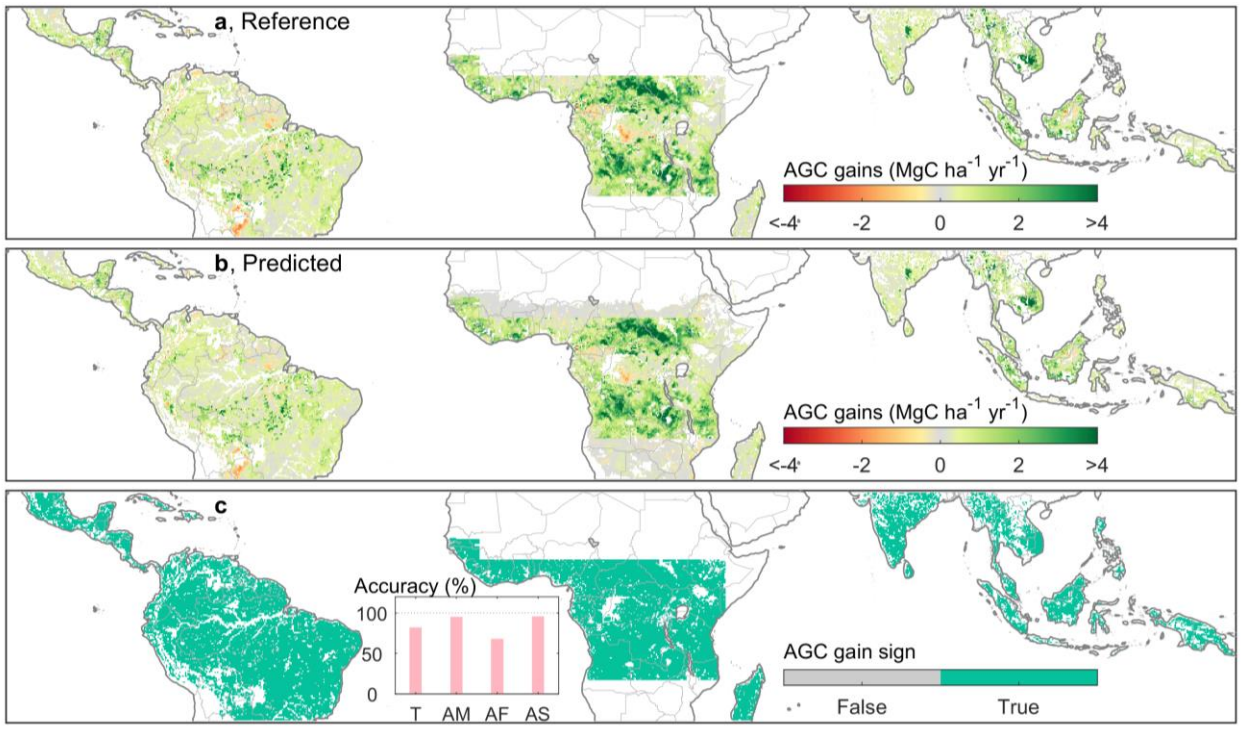

Fig. S11. Spatial patterns of trends in AGC gains from the reference and BRT model. a, AGC gains trends from the reference, **b** AGC gains trends from the BRT model. **c**, Accuracy of the BRT model for predicting the signs of AGC gains trends. In the inset of **c**, T, AM, AF, and AS denotes the tropics, tropical America, tropical Africa, and tropical Asia, respectively.

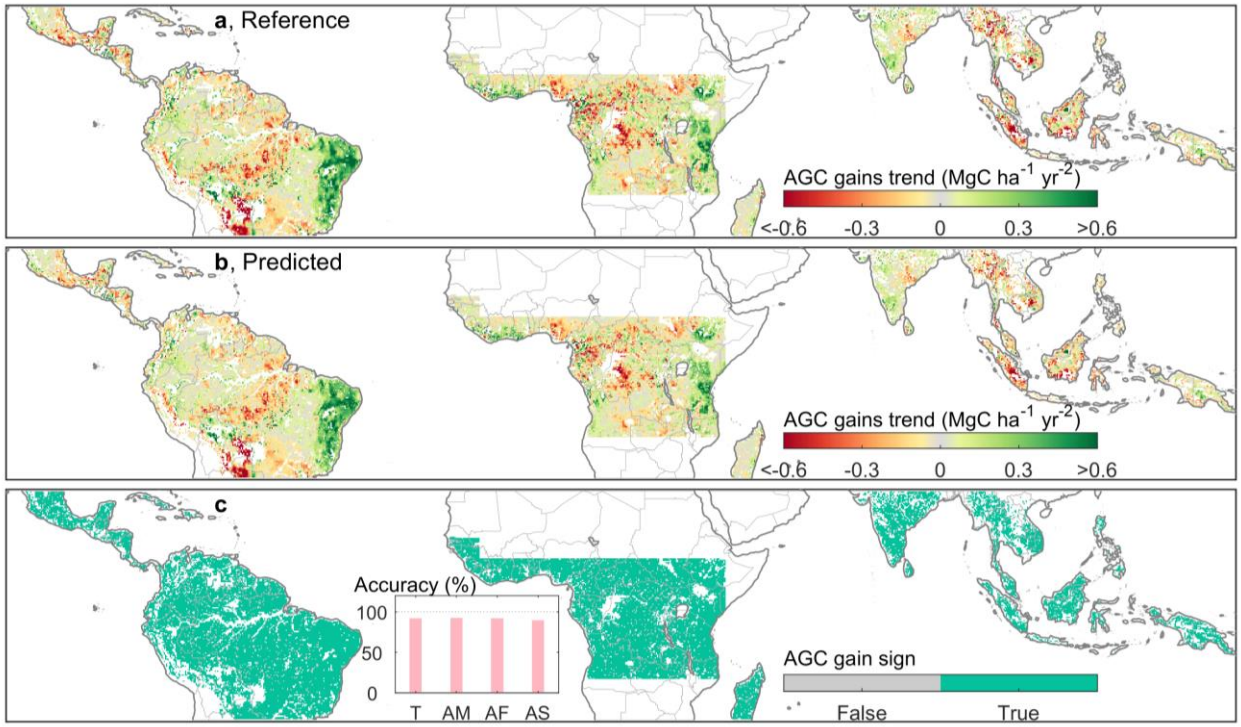

Fig. S12. Soil moisture comparison between ERA5-Land (ERA5-L) and another global 1km products (Zheng et al., 2023). (**a**) SM anomaly from 2010–2020. (**b**) Correlation coefficient between ERA5-L and Zheng at 0.25° cell. Dots indicate a significant correlation ($p < 0.05$). The p-values are calculated using a t-test.

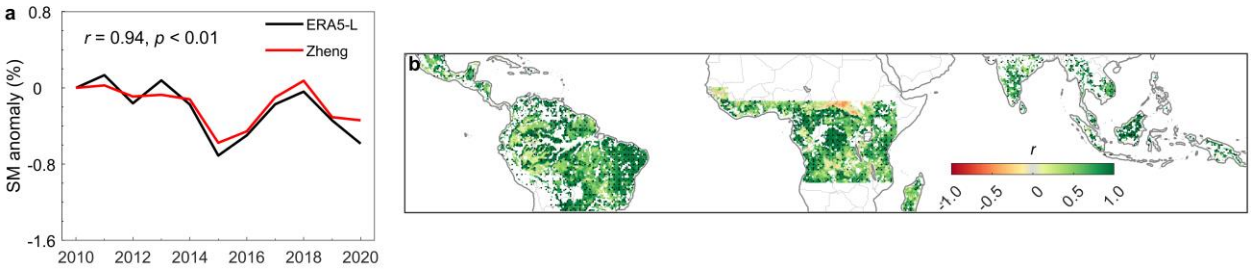

References:

Besnard, S., et al. Mapping global forest age from forest inventories, biomass and climate data. *Earth Syst. Sci. Data* **13**, 4881–4896 (2021).

Du, Z., et al. A global map of planting years of plantations. *Sci. Data* **9**, 141 (2022).

Hengl, T., et al. SoilGrids250m: Global gridded soil information based on machine learning. *PLoS One* **12**, e0169748 (2017).

Mu, H., et al. A global record of annual terrestrial Human Footprint dataset from 2000 to 2018. *Sci. Data* **9**, 176 (2022).

Olson, D. M., et al. Terrestrial Ecoregions of the World: A New Map of Life on Earth: A new global map of terrestrial ecoregions provides an innovative tool for conserving biodiversity. *BioScience* **51**, 933–938. (2001).

Ometto, J.P., et al. A biomass map of the Brazilian Amazon from multisource remote sensing. *Sci. Data* **10**, 668 (2023).

Potapov, P., et al. Mapping the world's intact forest landscapes by remote sensing. *Ecol. Soc.* **13**, 51 (2008).

Sabatini, F. M., et al. Global patterns of vascular plant alpha diversity. *Nat. Comm.* **13**, 4683. (2022).

Silva Junior, C. H., et al. Persistent collapse of biomass in Amazonian forest edges following deforestation leads to unaccounted carbon losses. *Sci. Adv.* **6**, eaax8360 (2020).

Yang, H., et al. Global increase in biomass carbon stock dominated by growth of northern young forests over past decade. *Nat. Geosci*. **16**, 886–892 (2023)

Zanaga, D., et al., 2021. ESA WorldCover 10 m 2020 v100. https://doi.org/10.5281/zenodo.5571936.

Zheng, C., et al. A 21-year dataset (2000–2020) of gap-free global daily surface soil moisture at 1-km grid resolution. *Sci. Data* **10**, 139 (2023).